INVERSE FILTERING IN THE PRESENCE OF DOPPLER WITH APPLICATION TO SPECULAR MULTIPATH PARAMETER ESTIMATION†

Mark D. Hahm, Edward L. Titlebaum and Zoran I. Mitrovski

Department of Electrical Engineering
University of Rochester
Rochester, NY 14627

ABSTRACT

It has been shown previously that, using a deconvolution method such as projection onto convex sets (POCS), which relies on some form of inverse filtering, one can increase the resolution of multipath parameter estimation in a Doppler environment beyond that which is achievable using correlation processing alone. This paper shows that the output of an inverse filter in the presence of Doppler can be characterized by two signal-related functions: one of which is free from the range-Doppler coupling effects inherent in correlation processing.

1. INTRODUCTION

Multipath parameter estimation is of interest in a number of communications applications [1]. The phenomenon of specular multipath occurs when a single transmitted signal arrives at the receiver via any combination of several distinct, unequal length paths. The received signal is not just the transmitted signal, but several delayed and amplitude-weighted versions of the original transmitted waveform, such that the multipath channel response, c(t), is modeled as having the form

$$c(t) = \sum_{k=1}^{N} \alpha_k \delta(t - \tau_k) \tag{1}$$

from which follows the form of the received signal, y(t):

$$y(t) = x(t) \otimes c(t) + n(t)$$

$$y(t) = \sum_{k=1}^{N} \alpha_k x(t - \tau_k) + n(t) \tag{2}$$

where N, α_k, and τ_k (k=1,2,...N) are the unknown multipath parameters, x(t) is the transmitted probing signal, n(t) is the channel noise, and $\otimes$ denotes convolution.

Within a radar or sonar environment, the multipath parameters may represent the number, cross-section, and range of targets within scanning range. In a communication environment, such as cellular radio, the multipaths from nearby buildings or geologic features can degrade system performance. However if the multipath parameters can be accurately determined, they can be used to enhance system performance by combining energy from multiple reflections to improve the effective SNR.

A first attempt at estimating the multipath parameters might be sending the received signal through a filter matched to the original transmitted waveform. In the absence of multipath, this does have the effect of maximizing the SNR, but time-bandwidth limitations of the original transmitted signal keep closely spaced specular reflections from being resolved in a multipath environment.

By using techniques other than elementary matched filtering, such as the method of projection onto convex sets (POCS) [2] or a least-squares (LS) estimation process [3], greater resolution between closely spaced paths can be attained over that which is achievable with matched filtering alone.

Thus far, this paper and the models discussed for channel multipath estimation have not considered the effects of Doppler. However, when there is motion of the receiver relative to the object that causes a particular specular multipath reflection, the previous model is inadequate. For the radar/sonar case, Doppler shift reveals the radial velocity of a target. For the communications case, Doppler can be another degrading effect. With Doppler included in the channel estimation problem, the new channel model, as a function of discrete time delay, t, and parametrized by Doppler shift, λ, becomes

$$c(t, \lambda) = \sum_{k=1}^{N} \alpha_k \delta(t - \tau_k, \lambda - \lambda_k) \tag{3}$$

and the received signal has the form

$$y(t) = \sum_{k=1}^{N} \alpha_k x(t - \tau_k) e^{j\lambda_k t} + n(t) \tag{4}$$

where λ_k is the unknown Doppler shift of the k^{th} multipath component and the narrow-band assumption for Doppler is made. To solve for N and the set of parameters

† This work was sponsored in part by the BMDO/IST and managed by the Office of Naval Research under contract N00014-92-J-1933 and in part by the AT&T Foundation through the Bell Laboratories PhD Scholar program.

0-7803-2431-5/95 $4.00

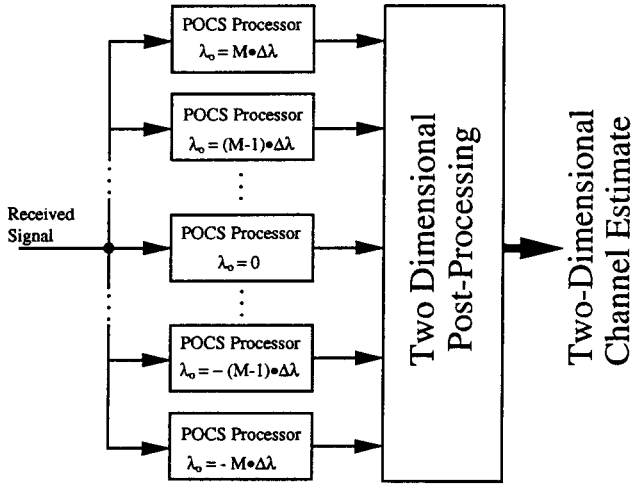

Figure 1 POCS Doppler Processing System

$$\{(\alpha_k, \tau_k, \lambda_k)\}$$

that characterize the multipath channel, a method was proposed in [4] that called for 2M+1 POCS processors running in parallel such that the m^{th} processor be tuned for highest response at an incremental Doppler shift of $m \bullet \Delta\lambda$ (m=-M, -M+1, ... -1, 0, 1, ... M-1, M). Here $\Delta\lambda$ determines the Doppler resolution of the system. A block diagram of the system is pictured in figure 1 and can be understood as a normal POCS processor (m=0) with 2M additional identical, but Doppler-shifted, POCS processors also working on the same received data. Sample outputs of the proposed system are pictured in figure 2. Similar outputs can be achieved by building an analogous system using LS estimation.

2. DOPPLER AND INVERSE FILTERING

The motivation for using deconvolution methods such as POCS or LS is rooted in the desire for greater time-delay resolution than is afforded by other means. Both POCS and LS reduce to inverse filtering when no channel noise is present. Thus if we wish to understand the output of POCS and LS in a system such as that in figure 2, we must characterize the output of an inverse filter (IF) in the presence of Doppler.

In the zero-Doppler case, the estimation of a *single* multipath component via inverse filtering follows from

$$C(\omega) = \frac{Y(\omega)}{X(\omega)} = \frac{\alpha_k X(\omega) e^{j\omega\tau_k}}{X(\omega)} = \alpha_k e^{j\omega\tau_k} \qquad (5)$$

and calculating the inverse Fourier transform gives

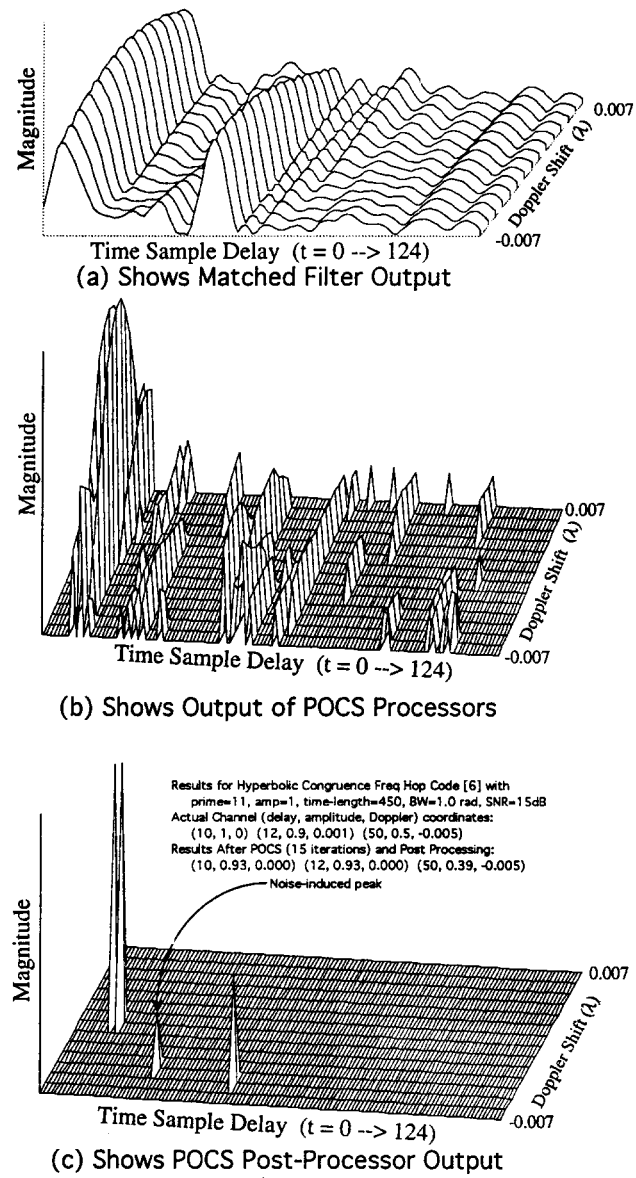

Figure 2

$$c(t) = \alpha_k \delta(t - \tau_k) \qquad (6)$$

where C(ω), Y(ω) and X(ω) denote the Fourier transforms of c(t), x(t), and y(t), respectively.

When Doppler is considered, however, the estimation of a single multipath component via inverse filtering is more complicated. By the system proposed in [4], the center frequency of a given processor element may not match the Doppler shift of a received multipath component. Observe that

$$C(\omega, \lambda_k) = \frac{Y(\omega)}{X(\omega)} = \frac{\alpha_k X(\omega - \lambda_k) e^{j\omega\tau_k}}{X(\omega)} \qquad (7)$$

Here λ_k can be interpreted as the Doppler mismatch between a processing element and the k^{th} received multipath component (e.g. if a component is Doppler shifted by 20Hz and the receiver element that processes it is centered around a Doppler shift of -10Hz, then $\lambda_k = 30$Hz). Of interest to us is the time domain representation of equation (7), but the form of this is not immediately clear. The factors α_k and $e^{j\omega\tau_k}$ contribute only to the scaling and delay estimation, respectively. Thus for Doppler estimation we are left with

$$\tilde{C}(\omega) = \frac{X(\omega - \lambda_k)}{X(\omega)} \qquad (8)$$

Equation (8) is the key to understanding the effect that a received Doppler-shifted signal will have on the output of a parallel processor element (that is part of a system as in figure 1) mismatched to the actual Doppler shift by an amount equal to λ_k. When the probing signal's spectrum, $X(\omega)$, has a zero crossing, equation (8) blows up for that particular value of ω. One might suggest constructing a signal that has no zeros in ω, but this is not possible; the zeros of $X(\omega)$ result from the finite time-length of x(t) and are located at predictable intervals of $2\pi/N$ radians on the ω axis, where N is the sampled-time-length of x(t). These zeros, in turn, cause poles to be placed at the same intervals along the ω axis of the IF's Fourier output (see figure 3).

A closed form solution for $\tilde{c}(t,\lambda_k)$, the inverse Fourier transform of (8), is difficult to obtain for most signals of interest. The following analysis shows, however, that for a large class of signals, $\tilde{c}(t,\lambda_k)$ may be approximated by a two-part model.

2.1 Ambiguity Function Effect

Consider equation (8) only in the range of $\omega_1 < \omega < \omega_2$ (where ω_1 and ω_2 are the 3dB points of $X(\omega)$). Also consider that, by multiplying the numerator and denominator by $X^*(\omega)$, (8) can be written as

$$\tilde{C}(\omega,\lambda_k) = \frac{X(\omega-\lambda_k)X^*(\omega)}{|X(\omega)|^2} = FT\left\{\chi^*_{xx}(-t,\lambda_k)\right\} \bullet W(\omega) \qquad (9)$$

where $\chi_{xx}(t,\lambda_k)$ is a slice of the auto-ambiguity function of x(t) (cf. [5]) parallel to the time axis, and $W(\omega)$ is the reciprocal of the power spectrum of x(t). Note that, in the range $[\omega_1,\omega_2]$, $W(\omega)$ is real and non-negative. It can be shown that if $X(\omega)$ is a wideband signal with a flat spectrum in the range $[\omega_1,\omega_2]$, then the time domain IF output attributed to this range of $\tilde{C}(\omega,\lambda_k)$ will be approximately

$$\tilde{c}(t,\lambda_k) \cong \beta \bullet \chi^*_{xx}(-t,\lambda_k) \qquad (10)$$

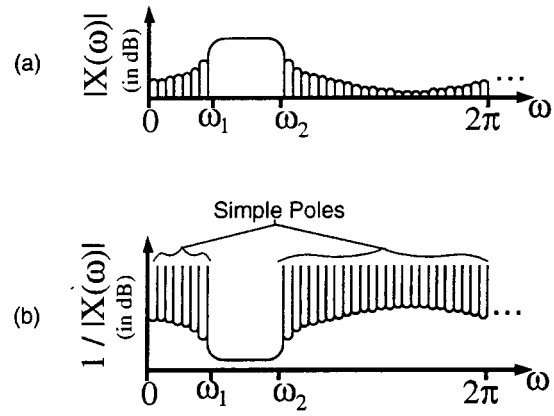

Figure 3

(a) shows the characteristics of a typical wideband probing signal's spectrum. Note the evenly spaced zeros. (b) shows what happens when $X(\omega)$ is inverted. Note the evenly spaced simple poles on the ω axis. The 3 dB points of $X(\omega)$ are also shown on the ω axes.

where

$$\beta = \frac{\omega_2 - \omega_1}{2\pi} = \frac{BW_X}{2\pi}$$

and BW_X is the 3dB bandwidth of $X(\omega)$.

2.2 Cosine Effect

Now consider (8) in the range outside of the interval $[\omega_1,\omega_2]$. The spectrum of the IF output in this range has poles at $2\pi/N$ intervals. This is due to the $\sin(N\omega/2)/\sin(\omega/2)$ spectral rolloff inherent in a signal with finite sampled-time-length N (see again figure 3a). Though the pole-filled figure 3b may look like a complicated spectrum, a good estimate of the inverse Fourier transform can be obtained through the application of Cauchy's integral formula. It can be shown that the contribution of the IF spectrum outside the range $[\omega_1,\omega_2]$ to the time domain estimate of the channel can be approximated as

$$\left|\tilde{c}(t,\lambda_k)\right| \cong \gamma \bullet \delta(t) \bullet \left|\cos\left(\frac{N}{2}\lambda_k\right)\right| \qquad (11)$$

where

$$\gamma = 1 - \frac{BW_X}{2\pi} = 1 - \beta$$

and. as before, BW_X is the 3dB bandwidth of $X(\omega)$.

2.3 Total Estimate of Inverse Filter Output

The chief assumption involved in the derivation of (10) and (11) is that of the flatness of $X(\omega)$ over some interval $[\omega_1,\omega_2]$. This assumption is valid for many probing signals of interest, including linear FM chirps and full frequency hop waveforms [6]. Combining the two equations gives:

$$\left|\tilde{c}(t,\lambda_k)\right| \cong (1-\beta)\bullet\delta(t)\bullet\left|\cos\left(\frac{N}{2}\lambda_k\right)\right| + \beta\bullet\left|\chi^*_{xx}(-t,\lambda_k)\right| \quad (12)$$

where β is as defined in (10). Note that (12) predicts the output of the IF in terms of things that we know or can calculate *a priori*. Note also that the cosine effect is free of range-Doppler coupling effects. In addition, for a given signal, we can trade off the ambiguity effect for the cosine effect, and vice versa, by increasing or decreasing the sampling rate of the system (decreasing or increasing β, respectively). When the sampling frequency is near the Nyquist rate, the ambiguity effect will dominate. When the received signal is sampled well above the Nyquist rate, the cosine effect will dominate. The output of an ensemble of inverse filters is shown in figure 4 for a chirp waveform with digital time-bandwidth product equal to 900 rad•samples (N=450, BW_X=2.0 radians).

3. CONCLUSION

The motivation for using inverse filtering is to accurately determine both the time delay and the Doppler shift of specular multipath components. From the preceding analysis, we conclude:

1.) The cosine effect is free of range-Doppler coupling effects. Thus the first term in (12) gives the accurate time delay estimate that we have sought and the shape of the inverse filter output along the Doppler axis at this delay. This information can be used to design the post-processor shown in figure 1 (since inverse filtering is used in POCS and LS). Because delay estimation is inherent in inverse filtering, the post processor primarily uses knowledge of the shape of the inverse filter output to determine the Doppler shift of each multipath component.

2.) The second term in (12) is a function of both delay and Doppler but is known before the signal is transmitted. Ideally one would like to minimize the ambiguity effect everywhere except at the (τ,λ) coordinates (0,0). Thus the second term advises that the signal be designed so that χ_{xx} have a small response away from the (τ,λ) origin --i.e. the classic thumbtack ambiguity function-- to minimize signal-induced artifacts in the IF output.

References

[1] B.P. Lathi, *Modern digital and analog communications systems*, HRW Saunders, USA, pp. 86-87, 1989.

[2] Z. Kostic', M.I. Sezan, and E.L. Titlebaum, "Estimation of the parameters of multipath channel using set-theoretic deconvolution", *IEEE Trans. on Comm.*, vol 40, pp. 1006-1011, June 1992.

[3] T.G. Manickam and R.J. Vaccaro, "A non-iterative deconvolution method for estimating multipath channel responses", *IEEE ICASSP Proc.*, I333-I336, 1993.

[4] M.D. Hahm and E.L. Titlebaum, "Multipath parameter estimation in the presence of doppler by the method of projection onto convex sets", *CISS Proc.*, Princeton, NJ, pp. 903-908, 1994.

[5] H.L. VanTrees, *Detection, Estimation, and Modulation Theory Vol III*, John Wiley and Sons, Inc, New York, pp. 279ff, 1971.

[6] S.V. Maric' and E.L. Titlebaum, "A class of frequency hop codes with nearly ideal charcteristics for use in multiple-access spread-spectrum communications and radar and sonar systems," *IEEE Trans. on Communications*, vol 40, pp. 1442-1447, Sept. 1992.

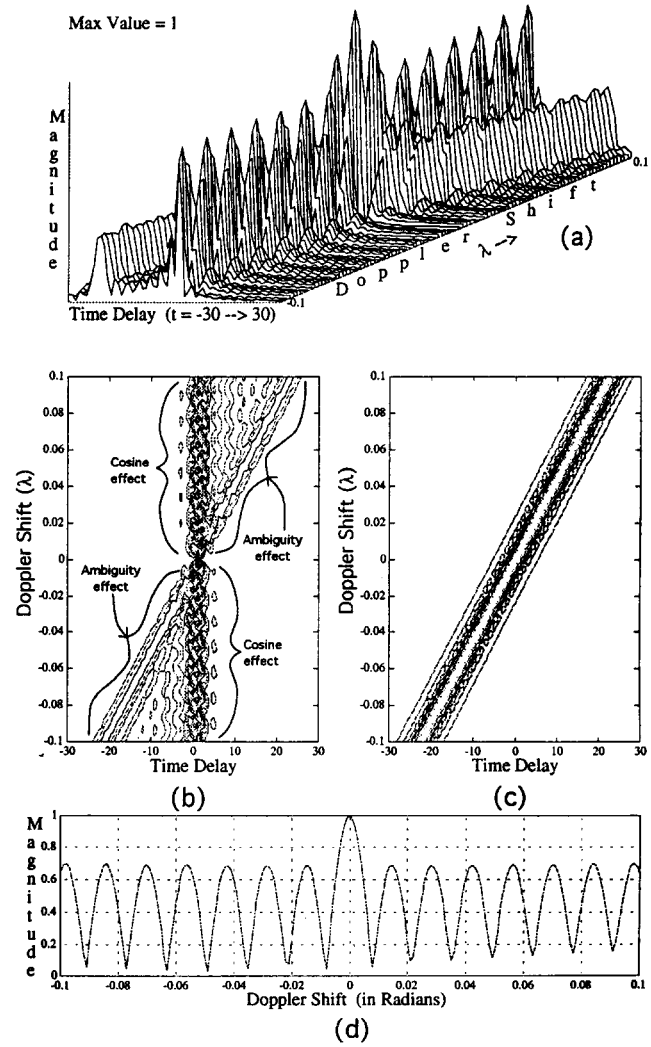

Figure 4

(a) and (b) are mesh and contour plots of the inverse filter output. (c) shows the contour plot of the probing signal's time-reversed auto-ambiguity function for comparison purposes. Note the center ridge of (a) and (b), demonstrating the range-Doppler coupling free component of inverse filtering due to the cosine effect. (d) shows a slice of (a) along the Doppler axis, clearly revealing the cosine effect along this axis, as predicted by (10) and (11).